TECHNISCHE MECHANIK
an open access journal

journal homepage: www.ovgu.de/techmech

Tech. Mech., Vol. 40, Is. 1, (2020), 22–30

Received: 28.09.2019
Accepted: 30.11.2019
Available online: 20.02.2020

Experimental and Numerical Investigation of the Material Behavior of semi-crystalline Polyamide 6

Sebastian Felder[1]*, Ngoc Anh Vu [2], Stefanie Reese[1], and Jaan-Willem Simon[1]

[1] RWTH Aachen University, Institute of Applied Mechanics (IFAM), Mies-van-der-Rohe-Str. 1, 52074 Aachen, Germany
[2] University of Twente, Department of Mechanics of Solids, Surfaces and Systems, P.O. box 217, 7500 AE Enschede, The Netherlands

Abstract: In the current work, the tensile properties of semi-crystalline Polyamide 6 are experimentally investigated for varying degrees of crystallinity, temperatures, and loading rates. Based on the experimental results, a phenomenological constitutive framework at finite strains is derived in a thermodynamically consistent manner. To this end, a hyperelastic-plastic intermolecular resistance and viscous molecular network resistance are considered. Non-linear kinematic and isotropic hardening as well as non-linear relaxation behavior are incorporated, to account for the experimentally observed behavior. It is evident that the mechanical behavior of semi-crystalline polymers exhibits complex dependencies on the degree of crystallinity and the temperature. To capture these experimental findings, both quantities serve as input parameters. A staggered parameter identification scheme is proposed to obtain a unique set of material parameters. Finally, the great capabilities of the proposed framework, to accurately predict the three-dimensional, visco-hyperelastic-plastic material response are demonstrated.

Keywords: semi-crystalline polymers, degree of crystallinity, hyperelastic-visco-plasticity, finite strains

1 Introduction

In contrast to thermoset polymers, which form irreversible chemical bonds throughout the curing process, thermoplastic polymers (TP) can undergo repeated heating above the melting point and cooling cycles. Consequently, TPs are well-suited for numerous technically relevant forming processes (e.g. extrusion or injection molding), where the polymer is reshaped into the desired geometry after heating. Semi-crystalline polymers (SCPs) represent a specific class of TPs, where the amorphous melt partly crystallize during the cooling phase. The resulting degree of crystallinity is in general depending on the processing conditions (e.g. the cooling rate, presence of moisture, and applied stress) cf. Fornes and Paul (2003). Naturally, the macroscopic material response is dictated by the underlying microstructure and is thus depending on the degree of crystallinity (see e.g. Jenkins (1992), Mohagheghian et al. (2015), and Ayoub et al. (2011)). SCPs can undergo large deformations and exhibit a complex visco-plastic material behavior (see e.g. Rae et al. (2007) and El-Qoubaa and Othman (2016)). In addition, significant thermo-mechanical coupling effects can be observed (i.e. the mechanical response is strongly influenced by the temperature and material self-heating occurs at higher loading rates, see e.g. Maurel-Pantel et al. (2015) and Parodi et al. (2018).
Due to this complex material behavior, a strong demand for computational models arises, which accurately predict the material and structural response of SCPs. Over the last decades, several constitutive frameworks, based on phenomenological modeling approaches on the continuum level (Srivastava et al. (2010), Ayoub et al. (2010), and Praud et al. (2017)) or exploiting multiscale modeling strategies (e.g. Li and Shojaei (2012) and Uchida and Tada (2013)), were proposed. Thermo-mechanically coupled models were developed among others by Maurel-Pantel et al. (2015) and Garcia-Gonzalez et al. (2017) for PA66 and PEEK, respectively. Despite the significant influence of the material internal microstructure (such as crystal volume fraction) on the effective material properties, only a limited number of authors accounted for this in their models. In the phenomenological model of Dusunceli and Colak (2008) and the formulation of Ayoub et al. (2011) and Abdul-Hameed et al. (2014), where the microstructure is represented by two-phases, the degree of crystallinity serves as a constant input parameter. However, in all these studies the effect of the degree of crystallinity was examined only for one specific temperature.
Over the last decades, numerous experimental investigations were published regarding the material behavior of SCPs. However, for Polyamide 6, which is the SCP of interest in the current work, the experimental data is scattered over the literature and, to the authors' knowledge, no comprehensive (true) stress stretch data, incorporating all of the following features, is available:

- Experimental investigation of the mechanical response for monotonic, cyclic, and relaxation test at finite strains;
- Consideration of a wide range of temperatures, spanning the glass transition temperature $\theta_g \approx 80$ °C;
- Accounting for different loading rates;
- Investigation of the influence of the crystallographic structure on the mechanical properties.

In the current work, an experimental approach is presented, in order to obtain a data base with the aforementioned characteristics. Based on these results, a phenomenological hyperelastic-visco-plastic constitutive framework is developed in a thermodynamically consistent manner. To capture the biphasic nature of the polymer and to account for different isothermal conditions, both the degree of crystallinity and temperature serve as input parameters. Finally, the model parameters are identified in a staggered procedure.

* E-mail address: sebastian.felder@rwth-aachen.de
doi: 10.24352/UB.OVGU-2020-010

First computations reveal the promising potential of this new model to accurately and efficiently predict the rate-dependent mechanical response for different degrees of crystallinity and at various temperatures.

2 Experimental investigation

Tensile experiments were conducted for Polyamide 6 (*Ultramid B40*, kindly provided by BASF SE). Dried specimens (type 5A in accordance with ISO 527-2:2012), produced by injection moulding, were tested in monotonic, cyclic, and relaxation tests at 22.4 °C, 50 °C, 120 °C, and 160 °C. To alter the initial degree of crystallinity χ_I= 23 %, annealing was applied for 5 hours at 180 °C, which resulted in a second set of specimens with χ_{II}= 28 %. In all experiments, the displacement of the cross head speed of the utilized *Zwick Z005* universal testing machine was prescribed and two different loading speeds (v_{min} = 1 mm/min and v_{max} = 10 mm/min) were investigated. The stretch field at the surface of the specimen was obtained by employing a 2D *ARAMIS 4M* digital image correlation (DIC) system. From the deformed cross section, the true stress in longitudinal x-direction σ_x was calculated. Noteworthy, only sections with almost constant stretch rates of $\dot{\lambda}_{x,min} \approx 0.0005$ s^{-1} and $\dot{\lambda}_{x,max} \approx 0.0058$ s^{-1} corresponding to v_{min} and v_{max}, were investigated.

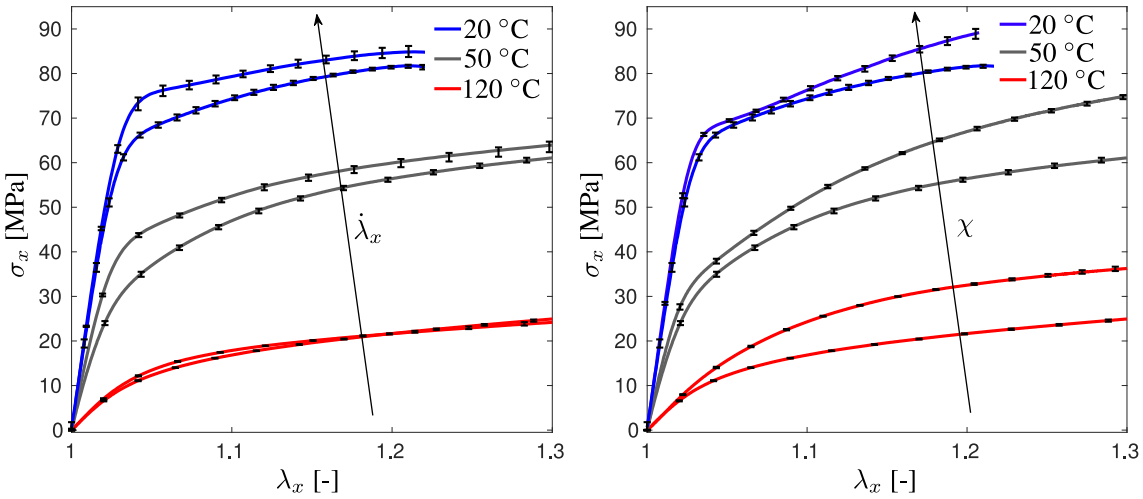

Fig. 1: Monotonic, uniaxial tensile tests at various temperatures: Effect of loading rate ($\dot{\lambda}_x$ = 0.0005 s^{-1} vs. $\dot{\lambda}_x$ = 0.0058 s^{-1}) for χ = 23 % (left). Effect of degree of crystallinity (χ = 23 % vs. χ = 28 %) for $\dot{\lambda}_x$ = 0.0005 s^{-1} (right).

In Figure 1 the longitudinal stress σ_x over stretch λ_x response for monotonic loading conditions is depicted. The significant influence of the temperature and degree of crystallinity on the rate dependent mechanical response was evident. Although the temperature on the surface of the specimens was not measured, self-heating of the material due to dissipative effects seemed to be present at higher loading rates and moderate stretch levels of $\lambda_1 \approx 1.07$ (already reported by e.g. Maurel-Pantel et al. (2015) and Parodi et al. (2018) for PA66 and PA6, respectively). At higher loading speeds, strain induced hardening competes with self-heating induced thermal-softening. This leads to a decrease of the slope of the stress-stretch curves and eventually to an intersection of the curves for v_{min} and v_{max} at higher temperatures (e.g. 120 °C).

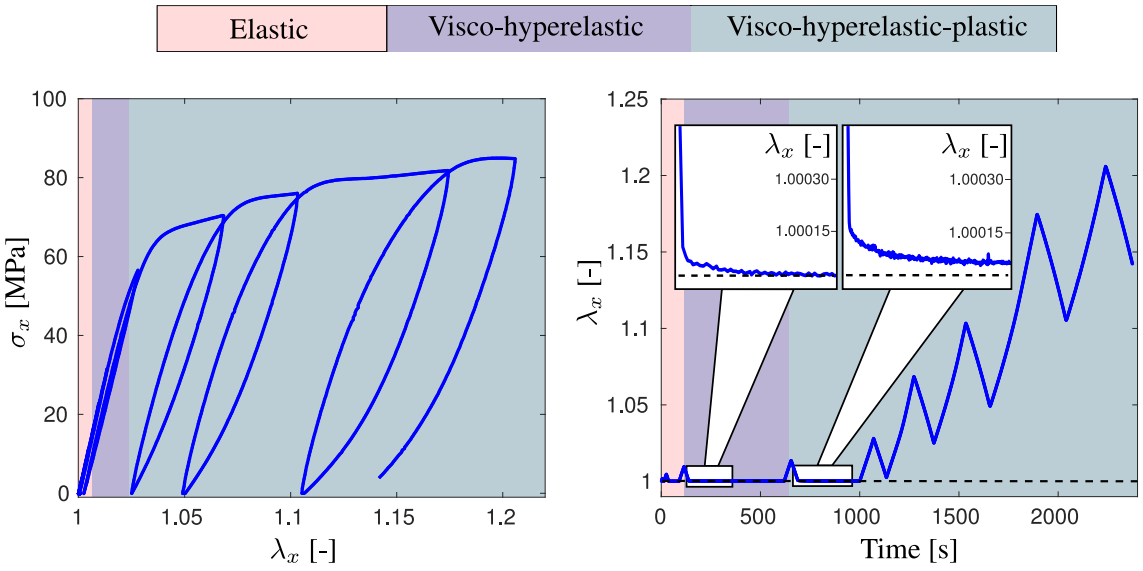

Fig. 2: Cyclic-loading-unloading-recovery experiment at room temperature

Cyclic-loading-unloading-recovery experiments were performed to reveal the complex deformation processes of the considered polymer. The stress over stretch and stretch over time relations are shown in Figure 2, for one exemplary cyclic experiment at room

temperature. Three distinct deformation regimes were observed: (i) In the elastic regime, the undeformed configuration (λ_x=1.0) was directly recovered after displacement controlled unloading to zero force. (ii) In the visco-hyperelastic regime, a remaining stretch level after unloading to zero force was present. However during the recovery step, where a zero force was prescribed, the remaining stretches were dissolved. (iii) In the visco-hyperelastic-plastic regime, the remaining stretch after unloading to zero force, converged towards an equilibrium plastic stretch level, at the end of the recovery step.
To assess the influence of the temperature and deformation level on the time-dependent material behavior, stepwise relaxation experiments were conducted. To this end, a loading speed of v_{max} = 10 mm/min was prescribed stepwise until a certain stretch level ($\lambda_x \approx 1.01$ and $\lambda_x \approx 1.15$) was reached. Subsequently, the displacement was held constant to allow for stress relaxation (see Figure 3). The data revealed a complex, non-linear dependency of the relaxation time on the stress and stretch level as well as on the temperature. This became more evident, by applying a post-processing scheme of the experimental data (see Section 4), which is founded on the proposed strategy of Amin et al. (2006).

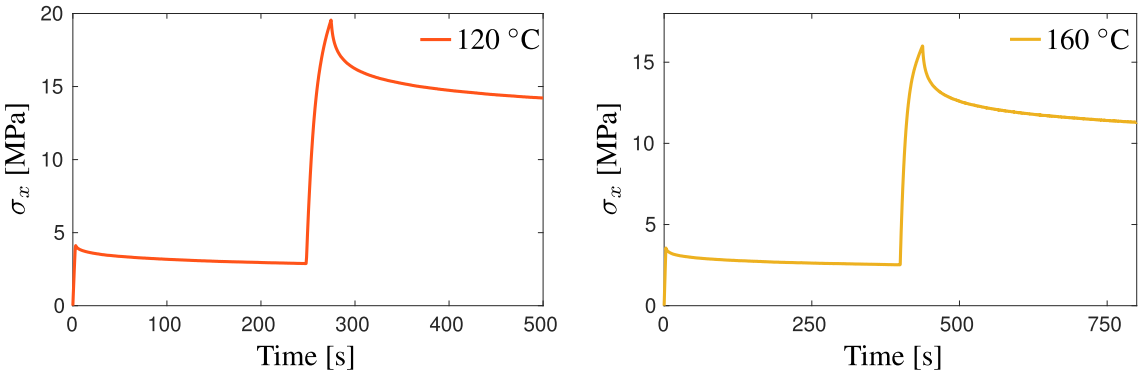

Fig. 3: Stepwise relaxation experiments at stretch levels of $\lambda_x \approx 1.01$ and $\lambda_x \approx 1.15$ at 120 °C and 160 °C

3 Material model formulation

In order to model the mechanical response of semi-crystalline PA6, the resistance of deformation is governed by a parallel arrangement of an intermolecular resistance and a molecular network resistance, in line with the contributions of e.g. Srivastava et al. (2010) and Ayoub et al. (2011). The intermolecular resistance is captured by means of an elasto-plastic model. To obtain the experimentally observed time dependent material behavior, the network resistance is represented by a viscous model to account for molecular orientation and relaxation. In the following, quantities associated with these resistances are distinguished by the subscripts $\mathfrak{m}$ (inter**m**olecular) and $\mathfrak{n}$ (molecular **n**etwork), respectively.

3.1 Multiplicative split of the deformation gradient

For the elasto-plastic model the classical multiplicative split of the total deformation gradient $\boldsymbol{F} = \boldsymbol{F}_{e\mathfrak{m}}\boldsymbol{F}_p$, into an elastic $\boldsymbol{F}_{e\mathfrak{m}}$ and plastic part $\boldsymbol{F}_p$ is proposed. Since, polymers exhibit a significant Bauschinger-like effect upon unloading (cf. e.g. Hasan and Boyce (1995) and Anand et al. (2009)), non-linear kinematic hardening of Frederick-Armstrong type is incorporated in the constitutive framework. To this end, a physically motivated (cf. Lion (2000)), additional multiplicative decomposition of the plastic part of the deformation gradient $\boldsymbol{F}_p = \boldsymbol{F}_{pe}\boldsymbol{F}_{pi}$, is employed. Furthermore, to model the viscous response of the SCP, a decomposition of the total deformation gradient $\boldsymbol{F} = \boldsymbol{F}_{e\mathfrak{n}}\boldsymbol{F}_i$, into an elastic $\boldsymbol{F}_{e\mathfrak{n}}$ and an inelastic part $\boldsymbol{F}_i$ is assumed (cf. Lubliner (1985) and Reese and Govindjee (1998)).

3.2 Constitutive relations and thermodynamic consistency

An additive split of the specific Helmholtz free energy into the contributions of the intermolecular and network resistance, denoted by $\psi_\mathfrak{m}$ and $\psi_\mathfrak{n}$, respectively, is proposed

$$\begin{aligned} \psi &= \psi_\mathfrak{m}(\boldsymbol{C}_{e\mathfrak{m}}, \boldsymbol{C}_{pe}, \kappa, \chi, \theta) + \psi_\mathfrak{n}(\boldsymbol{C}_{e\mathfrak{n}}, \chi, \theta) \\ \psi_\mathfrak{m} &= \psi_{e\mathfrak{m}}(\boldsymbol{C}_{e\mathfrak{m}}, \chi, \theta) + \psi_{kin}(\boldsymbol{C}_{pe}, \chi, \theta) + \psi_{iso}(\kappa, \chi, \theta) \end{aligned} \tag{1}$$

which depends on the deformation only through the right Cauchy-Green deformation tensors

$$\boldsymbol{C}_{e\mathfrak{m}} = \boldsymbol{F}_{e\mathfrak{m}}^T\boldsymbol{F}_{e\mathfrak{m}} = \boldsymbol{F}_p^{-T}\boldsymbol{C}\boldsymbol{F}_p^{-1}, \quad \boldsymbol{C}_{pe} = \boldsymbol{F}_{pe}^T\boldsymbol{F}_{pe} = \boldsymbol{F}_{pi}^{-T}\boldsymbol{C}_p\boldsymbol{F}_{pi}^{-1}, \quad \boldsymbol{C}_{e\mathfrak{n}} = \boldsymbol{F}_{e\mathfrak{n}}^T\boldsymbol{F}_{e\mathfrak{n}} = \boldsymbol{F}_i^{-T}\boldsymbol{C}\boldsymbol{F}_i^{-1} \tag{2}$$

based on the principle of material frame indifference. Here, $\boldsymbol{C} = \boldsymbol{F}^T\boldsymbol{F}$ is the right Cauchy-Green tensor and $\boldsymbol{C}_p = \boldsymbol{F}_p^T\boldsymbol{F}_p$ represents the plastic right Cauchy-Green tensor. In expression (1), the energy related to intermolecular reactions $\psi_{e\mathfrak{m}}$, the stored energy due to isotropic hardening ψ_{iso}, which is depending on the accumulated plastic strain κ, and a defect-energy associated with plastic deformations ψ_{kin} are introduced. The latter allows to phenomenologically account for the Bauschinger-like phenomena. Furthermore, all energy terms are assumed to depend on the degree of crystallinity χ and the temperature θ. Noteworthy, isothermal conditions ($\dot{\theta} = 0$) and no evolution of the crystalline phase ($\dot{\chi} = 0$) are assumed, such that χ and θ serve as input

parameters. With this new approach, the dependence of the effective material behavior on different crystal volume fractions (resulting from varying processing conditions) and different isothermal conditions is captured.
The constitutive equations are derived in a thermodynamically consistent manner from the Clausius-Duhem inequality

$$\boldsymbol{S} : \frac{1}{2}\dot{\boldsymbol{C}} - \rho_0 \dot{\psi} \geq 0 \tag{3}$$

which is here stated for isothermal processes, concomitant with the previous assumptions. The total second Piola-Kirchhoff stress tensor is denoted by $\boldsymbol{S}$ and ρ_0 is the density in the reference configuration. It is assumed that $\psi_{e\mathfrak{m}}$, $\psi_{e\mathfrak{n}}$, and ψ_{kin} are isotropic functions of $\boldsymbol{C}_{e\mathfrak{m}}$, $\boldsymbol{C}_{e\mathfrak{n}}$, and $\boldsymbol{C}_{pe}$, respectively. To obtain the constitutive relations, the total time derivative of the Helmholtz free energy (1) is inserted into the latter inequality and the following quantities are defined. The second Piola-Kirchhoff stress tensors

$$\boldsymbol{S}_{\mathfrak{m}} = 2\rho_0 \boldsymbol{F}_p^{-1} \frac{\partial \psi_{e\mathfrak{m}}}{\partial \boldsymbol{C}_{e\mathfrak{m}}} \boldsymbol{F}_p^{-T}, \quad \boldsymbol{S}_{\mathfrak{n}} = 2\rho_0 \boldsymbol{F}_i^{-1} \frac{\partial \psi_{\mathfrak{n}}}{\partial \boldsymbol{C}_{e\mathfrak{n}}} \boldsymbol{F}_i^{-T} \tag{4}$$

are corresponding to the intermolecular and molecular network resistance, respectively. The quantities

$$\boldsymbol{M}_{\mathfrak{m}} = 2\rho_0 \boldsymbol{C}_{e\mathfrak{m}} \frac{\partial \psi_{e\mathfrak{m}}}{\partial \boldsymbol{C}_{e\mathfrak{m}}}, \quad \boldsymbol{M}_{kin} = 2\rho_0 \boldsymbol{C}_{pe} \frac{\partial \psi_{kin}}{\partial \boldsymbol{C}_{pe}}, \quad \boldsymbol{M}_{\mathfrak{n}} = 2\rho_0 \boldsymbol{C}_{e\mathfrak{n}} \frac{\partial \psi_{\mathfrak{n}}}{\partial \boldsymbol{C}_{e\mathfrak{n}}} \tag{5}$$

represent symmetric stress tensors of Mandel-type and

$$\bar{\boldsymbol{X}} = 2\rho_0 \boldsymbol{F}_{pe} \frac{\partial \psi_{kin}}{\partial \boldsymbol{C}_{pe}} \boldsymbol{F}_{pe}^{T}, \quad R = -\rho_0 \frac{\partial \psi_{iso}}{\partial \kappa} \tag{6}$$

are the back stress tensor and the stress-like driving force of isotropic hardening, respectively. Following the standard arguments of Coleman and Noll (1961), the total second Piola-Kirchhoff stress tensor

$$\boldsymbol{S} = \boldsymbol{S}_{\mathfrak{m}} + \boldsymbol{S}_{\mathfrak{n}} \tag{7}$$

is obtained. Next, a yield function of von Mises type is assumed

$$\Phi = ||\mathrm{dev}(\boldsymbol{M}_{\mathfrak{m}}) - \mathrm{dev}(\bar{\boldsymbol{X}})|| - \sqrt{\frac{2}{3}}(\sigma_y - R) \tag{8}$$

where $||*||$ and $\mathrm{dev}(*)$ denote the Frobenius norm and the deviatoric part of a quantity, respectively, and the initial yield stress $\sigma_y(\chi, \theta)$ is introduced. In the following, $\boldsymbol{D}_{(*)} = \mathrm{sym}(\boldsymbol{L}_{(*)})$ is defined as the symmetric part of the corresponding velocity gradient $\boldsymbol{L}_{(*)} = \dot{\boldsymbol{F}}_{(*)} \boldsymbol{F}_{(*)}^{-1}$, with $(*) = i, p, pi$. The plastic flow rule and evolution equation for kinematic and isotropic hardening

$$\boldsymbol{D}_p = \dot{\gamma} \frac{\partial \Phi}{\partial \boldsymbol{M}_{\mathfrak{m}}} = \dot{\gamma} \frac{\mathrm{dev}(\boldsymbol{M}_{\mathfrak{m}}) - \mathrm{dev}(\bar{\boldsymbol{X}})}{||\mathrm{dev}(\boldsymbol{M}_{\mathfrak{m}}) - \mathrm{dev}(\bar{\boldsymbol{X}})||} \tag{9}$$

$$\boldsymbol{D}_{pi} = \dot{\gamma} \frac{b}{c} \mathrm{dev}(\boldsymbol{M}_{kin}) \tag{10}$$

$$\dot{\kappa} = \dot{\gamma} \frac{\partial \Phi}{\partial R} \tag{11}$$

corresponding to the intermolecular resistance, are derived in an associative manner. In the expression above the plastic multiplier $\dot{\gamma}$ was introduced. The evolution equation for kinematic hardening (10) is of Frederick-Armstrong type, where $b(\theta, \chi)$ and $c(\theta, \chi)$ are material parameters. Finally, the Kuhn-Tucker-conditions $\Phi \leq 0$, $\dot{\gamma} \geq 0$, and $\Phi \dot{\gamma} = 0$ supplement the elasto-plastic constitutive framework. The evolution of the inelastic deformation within the molecular network

$$\boldsymbol{D}_i = \frac{1}{2\tau\mu_{\mathfrak{n}}} \mathrm{dev}(\boldsymbol{M}_{\mathfrak{n}}) + \frac{1}{9\tau K_{\mathfrak{n}}} \mathrm{tr}(\boldsymbol{M}_{\mathfrak{n}}) \boldsymbol{I} \tag{12}$$

is chosen in line with the suggested form of Reese and Govindjee (1998). Here, the bulk modulus $K_{\mathfrak{n}}(\chi, \theta)$ and shear modulus $\mu_{\mathfrak{n}}(\chi, \theta)$, corresponding to the molecular network resistance are introduced. To model the relaxation behavior observed in experiments, the relaxation time τ is assumed to be a non-linear function of the overstress $\boldsymbol{S}_{\mathfrak{n}}$, the deformation and the temperature and is provided in Section 4.
This set of evolution equations (9)-(12) sufficiently satisfies the Clausius-Duhem inequality. For a detailed proof, the reader is referred to the works of Reese and Govindjee (1998) and Vladimirov et al. (2008).
All constitutive relations are derived with respect to several intermediate configurations. However, in order to implement the proposed framework as a material subroutine, tensorial pull back operations of the stress quantities $\boldsymbol{M}_{\mathfrak{m}}$, $\boldsymbol{M}_{kin}$, $\bar{\boldsymbol{X}}$, and $\boldsymbol{M}_{\mathfrak{n}}$ are performed, to represent all relations with respect to the reference configuration (see Table 1). As a result, the back stress tensor with respect to the reference configuration $\bar{\boldsymbol{X}}$ and the asymmetric stress like quantities $\boldsymbol{Y}$ and $\boldsymbol{Y}_{kin}$ are introduced (cf. Vladimirov et al. (2008)).
Up to now, no specific choices for the different free energy terms were made. Consequently, the proposed formulation offers great flexibility, since the relations for the thermodynamic driving forces have been derived in a completely general manner. For

Tab. 1: Constitutive equations with respect to the reference configuration

Intermolecular resistance	Molecular network resistance
Stresses $\boldsymbol{S}_{\mathfrak{m}} = 2\rho_0 \boldsymbol{F}_p^{-1} \frac{\partial \psi_{e\mathfrak{m}}}{\partial \boldsymbol{C}_{e\mathfrak{m}}} \boldsymbol{F}_p^{-T}$, $\tilde{\boldsymbol{X}} = 2\rho_0 \boldsymbol{F}_{pi}^{-1} \frac{\partial \psi_{kin}}{\partial \boldsymbol{C}_{pe}} \boldsymbol{F}_{pi}^{-T}$, $\boldsymbol{Y} = \boldsymbol{C}\boldsymbol{S}_{\mathfrak{m}} - \boldsymbol{C}_p\tilde{\boldsymbol{X}}, \quad \boldsymbol{Y}_{kin} = \boldsymbol{C}_p\tilde{\boldsymbol{X}}$, $R = -\rho_0 \frac{\partial \psi_{iso}}{\partial \kappa}$	**Stress** $\boldsymbol{S}_{\mathfrak{n}} = 2\rho_0 \boldsymbol{F}_i^{-1} \frac{\partial \psi_{\mathfrak{n}}}{\partial \boldsymbol{C}_{e\mathfrak{n}}} \boldsymbol{F}_i^{-T}$
Evolution equations $\dot{\boldsymbol{C}}_p = 2\dot{\gamma} \frac{\mathrm{dev}(\boldsymbol{Y})\boldsymbol{C}_p}{\sqrt{\mathrm{dev}(\boldsymbol{Y}) : \mathrm{dev}(\boldsymbol{Y})^T}}$, $\dot{\boldsymbol{C}}_{pi} = 2\dot{\gamma} \frac{b}{c} \mathrm{dev}(\boldsymbol{Y}_{kin})\boldsymbol{C}_{pi}, \quad \dot{\kappa} = \sqrt{\frac{2}{3}}\dot{\gamma}$	**Evolution equation** $\dot{\boldsymbol{C}}_i = \left(\frac{1}{\tau\mu_{\mathfrak{n}}} \mathrm{dev}(\boldsymbol{C}\boldsymbol{S}_{\mathfrak{n}}) + \frac{2}{9\tau K_{\mathfrak{n}}} \mathrm{tr}(\boldsymbol{C}\boldsymbol{S}_{\mathfrak{n}})\boldsymbol{I} \right) \boldsymbol{C}_i$
Yield function $\Phi = \sqrt{\mathrm{dev}(\boldsymbol{Y}) : \mathrm{dev}(\boldsymbol{Y})^T} - \sqrt{\frac{2}{3}}(\sigma_y - R)$	
Kuhn-Tucker-conditions $\Phi \leq 0$, $\dot{\gamma} \geq 0$, and $\Phi\dot{\gamma} = 0$	
Second Piola-Kirchhoff stress $\boldsymbol{S} = \boldsymbol{S}_{\mathfrak{m}} + \boldsymbol{S}_{\mathfrak{n}}$	

the intermolecular resistance, a Neo-Hookean material with combined linear and non-linear isotropic hardening of Voce type is assumed. The corresponding volumetric energy terms Ψ read

$$\Psi_{e\mathfrak{m}} = \frac{\mu_{\mathfrak{m}}}{2} (\mathrm{tr}(\boldsymbol{C}_{e\mathfrak{m}}) - 3) - \mu_{\mathfrak{m}} \ln(J_{e\mathfrak{m}}) + \frac{\Lambda_{\mathfrak{m}}}{4} (\det(\boldsymbol{C}_{e\mathfrak{m}}) - 1 - 2\ln(J_{e\mathfrak{m}})) \tag{13}$$

$$\Psi_{kin} = \frac{c}{2}(\mathrm{tr}(\boldsymbol{C}_{pe}) - 3) - c\ln(J_{pe}) \tag{14}$$

$$\Psi_{iso} = (\sigma_\infty - \sigma_y)\left(\kappa + \frac{\exp(-\beta\kappa)}{\beta}\right) + \frac{1}{2}H\kappa^2 \tag{15}$$

Here, the Lamé constants and isotropic hardening parameters are defined by $\mu_{\mathfrak{m}}(\theta, \chi)$, $\Lambda_{\mathfrak{m}}(\theta, \chi)$, $\sigma_\infty(\theta, \chi)$, $\beta(\theta, \chi)$, and $H(\theta, \chi)$, respectively. Furthermore, the identities $J_{e\mathfrak{m}} = \det\boldsymbol{F}_{e\mathfrak{m}}$ and $J_{pe} = \det\boldsymbol{F}_{pe}$ are introduced. For simplicity, the elastic energy contribution of the molecular network resistances is chosen to be of Neo-Hookean type as well, namely

$$\Psi_{\mathfrak{n}} = \frac{\mu_{\mathfrak{n}}}{2} (\mathrm{tr}(\boldsymbol{C}_{e\mathfrak{n}}) - 3) - \mu_{\mathfrak{n}} \ln(J_{e\mathfrak{n}}) + \frac{\Lambda_{\mathfrak{n}}}{4} (\det(\boldsymbol{C}_{e\mathfrak{n}}) - 1 - 2\ln(J_{e\mathfrak{n}})) \tag{16}$$

where the Lamé constants corresponding to the molecular network resistance are represented by $\mu_{\mathfrak{n}}(\chi, \theta)$ and $\Lambda_{\mathfrak{n}}(\chi, \theta)$, respectively and $J_{e\mathfrak{n}} = \det\boldsymbol{F}_{e\mathfrak{n}}$ holds. It is assumed that the material parameters are functions of the temperature and total degree of crystallinity, to capture the experimentally observed dependency of the macroscopic material response on these quantities. The specific relations are provided in Section 4.

The algorithmic treatment of the constitutive equations corresponding to the elasto-plastic model is based on the proposed strategy by Dettmer and Reese (2004) and Vladimirov et al. (2008). The numerical time integration and solution procedure for the evolution equation of the viscous model is adopted from Reese and Govindjee (1998). These are not further discussed in the current work.

4 Material parameter characterization

The material parameters were obtained from the experimental results discussed in Section 2. A staggered parameter identification procedure was developed to obtain a unique set of parameters for each temperature separately.

1. The elastic constants were governed from the material response under monotonic tension in the elastic deformation regime (cf. Section 2). The Poisson's ratio of intermolecular and molecular network resistance were assumed to be equal (i.e. $\nu_{\mathfrak{m}} = \nu_{\mathfrak{n}}$) and were calculated from the negative ratio of the transverse and longitudinal stretch data. The Young's moduli $E_{\mathfrak{m}}$ and $E_{\mathfrak{n}}$ were governed from the initial stiffness of PA6 for different degrees of crystallinity. For simplicity, it was assumed that only the stiffness of the intermolecular resistance depends linearly on χ.

2. In the second identification step, the function for the relaxation time τ was determined, based on the relaxation data for different stretch levels. To this end, a post-processing scheme for the recorded stress relaxation data, which was originally proposed by Amin et al. (2006), was utilized to assess the influence of the temperature and overstress and stretch level on the evolution of the relaxation time. A non-linear relation was evident at higher stretch levels, in contrast to a almost linear relation at small stretches (exemplary depicted in Figure 4 for relaxation data at 120 °C). To capture the evolution of the relaxation time, the following function was assumed

$$\tau = \tau_0 \frac{||\boldsymbol{C}||_s^{\varphi}}{\exp(||\boldsymbol{\sigma}_{\mathrm{n}}||_s)^{\delta}} \tag{17}$$

In the expression above $||*||_s$ is defined as the second norm of a tensor (i.e. $||*||_s = \sqrt{\omega_{\max}}$, with $\omega_{\max}$ being the maximum eigenvalue of $(*)^T(*)$) and $\boldsymbol{\sigma}_{\mathrm{n}}$ represents the Cauchy stress corresponding to the molecular network resistance.

The additional material parameters $\tau_0(\theta)$, $\varphi(\theta)$, and $\delta(\theta)$ were obtained by simultaneously minimizing the summed square of residuals (defined as the difference between the observed experimental data and fitted model response) for different stretch levels. To this end, the Trust-region algorithm, which is provided as an intrinsic functions in the commercial software *MATLAB*, was utilized without introducing additional scale (weight) factors. Noteworthy, with the proposed nonlinear function for the relaxation time (17), a better fit for the nonlinear evolution at higher stretch levels was achieved (cf. Figure 4). The comparatively weak fit at small stretches might be improved by introducing additional material parameters. However, it should be emphasized that the visco-elastic material response was accurately captured with this choice of constitutive equation and corresponding set of parameters (see Section 5).

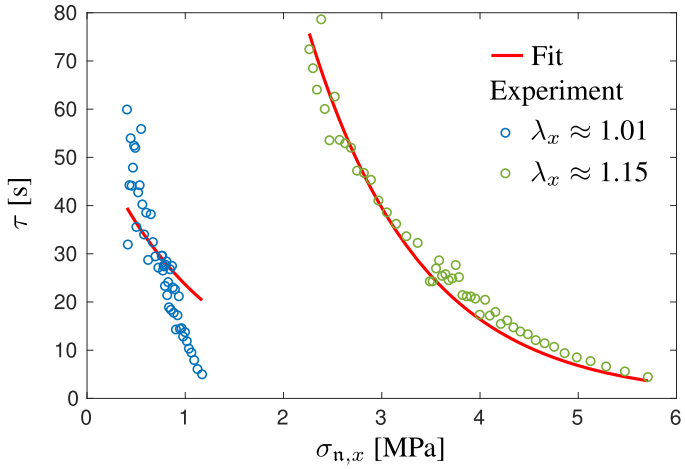

Fig. 4: Relaxation time overstress relation: Experimental data and corresponding fit for different λ_x at 120 °C and χ_I.

3. The initial yield stress $\sigma_y(\chi, \theta)$ was directly obtained from the onset of yield, which was determined from the cyclic experiments for different degrees of crystallinity.
4. Due to the lack of cyclic tension compression data, kinematic hardening was neglected by setting the corresponding parameter c to zero. Finally, the isotropic hardening parameters (i.e $\beta(\theta, \chi)$, $\sigma_\infty(\theta, \chi)$, and $H(\theta, \chi)$) were obtained from the monotonic tensile test data, by simultaneously minimizing the least-square residuals of the 3D stress-stretch response for different loading rates and degrees of crystallinity.

Tab. 2: Set of mechanical parameters for 120 °C

$E_{\mathrm{m}} = \chi E_{\mathrm{m}}^0(\theta)$	$E_{\mathrm{n}} = E_{\mathrm{n}}(\theta)$	$\nu_{\mathrm{m,n}}(\theta)$	$\sigma_y = \chi\sigma_y^0(\theta)$	$\beta = \chi\beta_0(\theta)$	$H = \chi H_0(\theta)$	$\sigma_\infty = \chi^{\alpha(\theta)}\sigma_\infty^0(\theta)$	$\tau(\boldsymbol{\sigma}_{\mathrm{n}}, \boldsymbol{C}, \theta)$ cf. (17)
E_{m}^0: 1050 [MPa]	E_{n}: 201 [MPa]	0.35 [-]	σ_y^0: 30 [MPa]	β_0: 228 [-]	H_0: 215 [MPa]	σ_∞^0: 1253 [MPa]	τ_0: 48 [s]
						α: 3.061 [-]	φ: 2.38 [-]
							δ: 0.714 [-]

Up to now, the staggered parameter identification procedure was only conducted for 120 °C (corresponding set of parameters see Table 2), where all required experimental data was already available. However, the general procedure is suited for all other considered temperatures and will lead to equivalent results.

The corresponding stress over stretch response of the model was well fitted to the experimental data (see Figure 5). Noteworthy, due to the material self-heating at higher loading rates (cf. Section 2), the isothermal model ($\dot{\theta} = 0$) was only calibrated up to stretch levels of $\lambda_x = 1.07$ for $\dot{\lambda}_{x,max} \approx 0.0058$ s^{-1}. Consequently, the model response leads to an overestimation of the stress after this stretch level for the higher loading rate. To capture the phenomenon of material self-heating and corresponding thermal-softening correctly, a fully thermo-mechanically-coupled model formulation needs to be developed in the future.

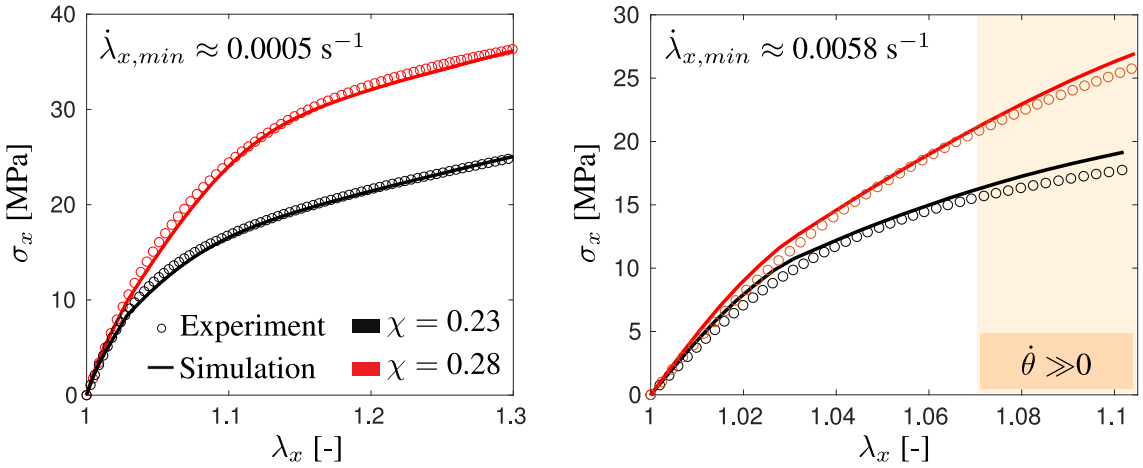

Fig. 5: Monotonic, uniaxial extension - Experimental data and corresponding model fit at 120 °C

5 Model verification

In order to verify, the obtained parameters, the model response was evaluated for the cyclic loading-unloading-recovery procedure and compared with the experimental data. To this end, the proposed theory was implemented as a user material subroutine *UMAT* into the commercial FEM software *ABAQUS*/Standard and a single element test was considered. The stress in longitudinal x-direction obtained from the experimental data as a function of time was prescribed as a traction boundary condition. The resulting stress over stretch response is in excellent agreement with the experimental records (see Figure 6 on the left).
Furthermore, the recorded stretch in transversal y-direction over time was compared with the model response (see Figure 6 on the right). The latter results emphasized the great capabilities of the proposed constitutive framework to accurately predict the three-dimensional, visco-hyperelastic-plastic material response of Polyamide 6 at large deformations ($\lambda_x > 1.4$).

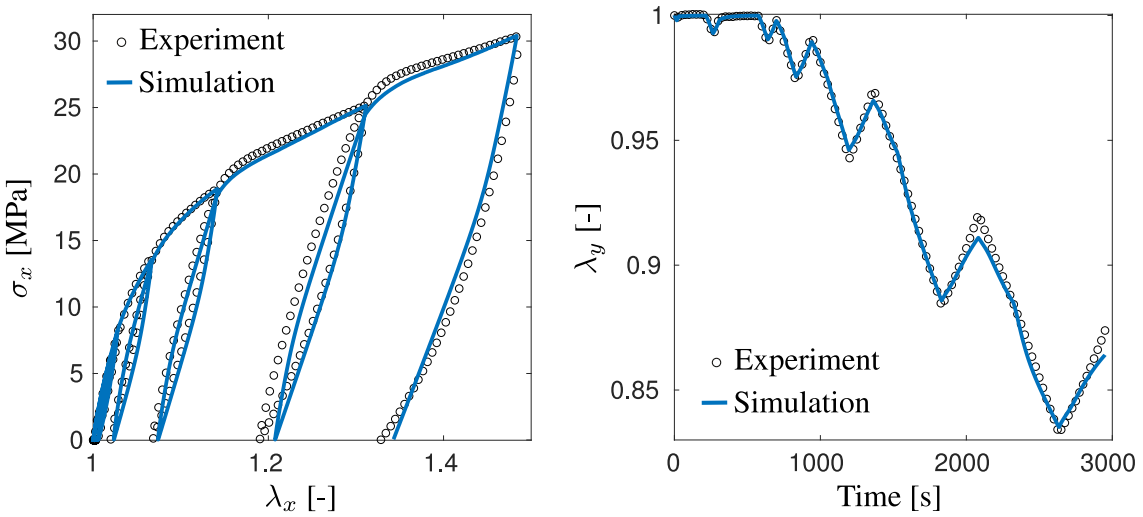

Fig. 6: Experimental data and corresponding model prediction for cyclic loading-unloading-recovery procedure at 120 °C and χ_I: Longitudinal stress σ_x over stretch λ_x response (left). Transversal stretch λ_y over time (right).

6 Conclusion

In the current work, a constitutive framework was proposed for analyzing, predicting, and optimizing the material and structural response of semi-crystalline polymers. This new theory was founded on a preceding comprehensive experimental study, where particular attention was paid on investigating the material response of semi-crystalline Polyamide 6 over a wide range of temperatures and for different degrees of crystallinity. The experimental observations provided important insights into the complex dependencies of the effective material properties on the aforementioned factors and revealed three distinct deformation regimes (i.e. elastic, visco-hyperelastic, and visco-hyperelastic-plastic regime).
Based on these results, a material model, which is valid for finite strains, was developed in a thermodynamically consistent manner. To phenomenologically capture the observed deformation regimes, a parallel arrangement of an elasto-plastic and viscous model was proposed. Furthermore, to account for the significant influence of the temperature and degree of crystallinity on the mechanical response, both quantities served as model inputs. The material parameters were obtained from a staggered identification procedure, which was performed up to now only for 120 °C, due to the lack of a complete experimental database. However, first computational results demonstrated the great capabilities of the proposed framework, to accurately predict the

three-dimensional, visco-hyperelastic-plastic material response of Polyamide 6 at large deformations.
To fully characterize and validate the constitutive framework in the future, much work needs to be done. First of all, the experimental study must be completed for all considered temperatures. Based on these results, the proposed parameter identification procedure can be applied in a straight forward manner and will lead to a set of material parameters for each temperature. Of particular interest is, in addition, the investigation of stress relaxation for different degrees of crystallinity, which is not incorporated in the model yet. To improve the models capabilities in the context of more complex multidimensional stress states, additional shear-, compression- and combined loading procedures need to be conducted. Furthermore, to characterize the kinematic hardening response, combined tension-compression experiments are required. Based on these results, the energy contributions and yield surface can be adjusted in a straight forward manner, due to the general derivation of the proposed model and corresponding high flexibility.
Moreover, infrared thermography measurements should be performed during testing to confirm the material self-heating at higher loading rates. These results and the set of material parameters at different temperatures will provide an important foundation for a thermo-mechanically coupled model formulation.

Acknowledgments

Financial support of the projects RE 1057/41 and RE 1057/46 by the German Science Foundation (DFG) is gratefully acknowledged. Furthermore, the authors are grateful for the provision of *Ultramid B40* by BASF SE and for the production of the tensile specimen by the "Institut für Textiltechnik" (ITA) of RWTH Aachen University.

References

H. Abdul-Hameed, T. Messager, F. Zaïri, and M. Naït-Abdelaziz. Large-strain viscoelastic-viscoplastic constitutive modeling of semi-crystalline polymers and model identification by deterministic/evolutionary approach. *Computational Materials Science*, 90:241 – 252, 2014. doi: https://doi.org/10.1016/j.commatsci.2014.03.043.

A. F. M. S. Amin, A. Lion, S. Sekita, and Y. Okui. Nonlinear dependence of viscosity in modeling the rate-dependent response of natural and high damping rubbers in compression and shear: Experimental identification and numerical verification. *International Journal of Plasticity*, 22(9):1610 – 1657, 2006. doi: https://doi.org/10.1016/j.ijplas.2005.09.005.

L. Anand, N. M. Ames, V. Srivastava, and S. A. Chester. A thermo-mechanically coupled theory for large deformations of amorphous polymers. part i: Formulation. *International Journal of Plasticity*, 25(8):1474 – 1494, 2009. ISSN 0749-6419. doi: https://doi.org/10.1016/j.ijplas.2008.11.004.

G. Ayoub, F. Zaïri, M. Naït-Abdelaziz, and J. M. Gloaguen. Modelling large deformation behaviour under loading - unloading of semicrystalline polymers: Application to a high density polyethylene. *International Journal of Plasticity*, 26(3):329 – 347, 2010. doi: https://doi.org/10.1016/j.ijplas.2009.07.005.

G. Ayoub, F. Zaïri, C. Fréderix, J.M. Gloaguen, M. Naït-Abdelaziz, R. Seguela, and J.M. Lefebvre. Effects of crystal content on the mechanical behaviour of polyethylene under finite strains: Experiments and constitutive modelling. *International Journal of Plasticity*, 27(4):492 – 511, 2011. doi: https://doi.org/10.1016/j.ijplas.2010.07.005.

B. D. Coleman and W. Noll. Foundations of linear viscoelasticity. *Reviews of Modern Physics*, 33:239–249, Apr 1961. doi: 10.1103/RevModPhys.33.239.

W. Dettmer and S. Reese. On the theoretical and numerical modelling of Armstrong-Frederick kinematic hardening in the finite strain regime. *Computer Methods in Applied Mechanics and Engineering*, 193(1 – 2):87 – 116, 2004. doi: 10.1016/j.cma.2003.09.005.

N. Dusunceli and O. U. Colak. Modelling effects of degree of crystallinity on mechanical behavior of semicrystalline polymers. *International Journal of Plasticity*, 24(7):1224 – 1242, 2008. doi: https://doi.org/10.1016/j.ijplas.2007.09.003.

Z. El-Qoubaa and R. Othman. Strain rate sensitivity of polyetheretherketone's compressive yield stress at low and high temperatures. *Mechanics of Materials*, 95:15 – 27, 2016. doi: https://doi.org/10.1016/j.mechmat.2015.12.008.

T.D. Fornes and D.R. Paul. Crystallization behavior of nylon 6 nanocomposites. *Polymer*, 44(14):3945 – 3961, 2003. doi: https://doi.org/10.1016/S0032-3861(03)00344-6.

D. Garcia-Gonzalez, R. Zaera, and A. Arias. A hyperelastic-thermoviscoplastic constitutive model for semi-crystalline polymers: Application to peek under dynamic loading conditions. *International Journal of Plasticity*, 88:27 – 52, 2017. doi: https://doi.org/10.1016/j.ijplas.2016.09.011.

O. A. Hasan and M. C. Boyce. A constitutive model for the nonlinear viscoelastic viscoplastic behavior of glassy polymers. *Polymer Engineering & Science*, 35(4):331 – 344, 1995. doi: 10.1002/pen.760350407.

A. D. Jenkins. *Polymers: chemistry & physics of modern materials*, volume 28. J. M. G. Cowie Blackie & Son Ltd, Glasgow & London Chapman & Hall, New York, 1991, 1992. doi: 10.1002/pi.4990280115.

G. Li and A. Shojaei. A viscoplastic theory of shape memory polymer fibres with application to self-healing materials. *Proceedings of the Royal Society A: Mathematical, Physical and Engineering Sciences*, 468(2144):2319 – 2346, 2012. doi: 10.1098/rspa.2011.0628.

A. Lion. Constitutive modelling in finite thermoviscoplasticity: a physical approach based on nonlinear rheological models. *International Journal of Plasticity*, 16(5):469 – 494, 2000. doi: 10.1016/S0749-6419(99)00038-8.

J. Lubliner. A model of rubber viscoelasticity. *Mechanics Research Communications*, 12(2):93 – 99, 1985. doi: https://doi.org/10.1016/0093-6413(85)90075-8.

A. Maurel-Pantel, E. Baquet, J. Bikard, J. L. Bouvard, and N. Billon. A thermo-mechanical large deformation constitutive model for polymers based on material network description: Application to a semi-crystalline polyamide 66. *International Journal of Plasticity*, 67:102 – 126, 2015. doi: https://doi.org/10.1016/j.ijplas.2014.10.004.

I. Mohagheghian, G. J. McShane, and W. J. Stronge. Impact perforation of monolithic polyethylene plates: Projectile nose shape dependence. *International Journal of Impact Engineering*, 80:162 – 176, 2015. doi: https://doi.org/10.1016/j.ijimpeng.2015.02.002.

E. Parodi, P. W. M. Gerrit, and L. E. Govaert. Prediction of plasticity-controlled failure in polyamide 6: Influence of temperature and relative humidity. *Journal of Applied Polymer Science*, 135(11):45942, 2018. doi: 10.1002/app.45942.

F. Praud, G. Chatzigeorgiou, J. Bikard, and F. Meraghni. Phenomenological multi-mechanisms constitutive modelling for thermoplastic polymers, implicit implementation and experimental validation. *Mechanics of Materials*, 114:9 – 29, 2017. doi: https://doi.org/10.1016/j.mechmat.2017.07.001.

P. J. Rae, E. N. Brown, and E. B. Orler. The mechanical properties of poly(ether-ether-ketone) (peek) with emphasis on the large compressive strain response. *Polymer*, 48(2):598 – 615, 2007. doi: https://doi.org/10.1016/j.polymer.2006.11.032.

S. Reese and S. Govindjee. A theory of finite viscoelasticity and numerical aspects. *International Journal of Solids and Structures*, 35(26):3455 – 3482, 1998. doi: https://doi.org/10.1016/S0020-7683(97)00217-5.

V. Srivastava, S. A. Chester, N. M. Ames, and L. Anand. A thermo-mechanically-coupled large-deformation theory for amorphous polymers in a temperature range which spans their glass transition. *International Journal of Plasticity*, 26(8):1138 – 1182, 2010. doi: https://doi.org/10.1016/j.ijplas.2010.01.004. Special Issue In Honor of Lallit Anand.

M. Uchida and N. Tada. Micro-, meso- to macroscopic modeling of deformation behavior of semi-crystalline polymer. *International Journal of Plasticity*, 49:164 – 184, 2013. doi: https://doi.org/10.1016/j.ijplas.2013.03.007.

I. N. Vladimirov, M. P. Pietryga, and S. Reese. On the modelling of non-linear kinematic hardening at finite strains with application to springback – comparison of time integration algorithms. *International Journal for Numerical Methods in Engineering*, 75 (1):1 – 28, 2008. doi: 10.1002/nme.2234.